Contrasting sensitivity of weathering proxies to Quaternary climate and sea level fluctuations in the southern South China Sea

Yi Zhong[1], David Wilson[2], Jiabo Liu[3], Shiming Wan[4], Rui Bao[5], Jianxing Liu[6], Yanan Zhang[7], Xuesong Wang[8], Yuanhao Liu[7], Xiaoyu Liu[7], Ying Zhao[7], and Qingsong Liu[9]

[1]Department of Marine Science and Engineering, Southern University of Science and Technology,
[2]University College London
[3]Center for Marine Magnetism, Department of Ocean Science and Engineering, Southern University of Science and Technology
[4]Institute of Oceanology, Chinese Academy of Sciences
[5]ETH Zurich
[6]First Institute of Oceanography,Ministry of Natural Resources (MNR) , China
[7]Center for Marine Magnetism (CM2), Department of Ocean Science and Engineering, Southern University of Science and Technology, Shenzhen 518055, PR China
[8]Key Laboratory of Ocean and Marginal Sea Geology, South China Sea Institute of Oceanology, Chinese Academy of Sciences
[9]South University of Science and Technology of China

November 21, 2022

Abstract

Tropical marginal seas host unique sedimentary archives that may be exploited to reveal past changes in continental erosion, chemical weathering, and ocean dynamics. However, these records can be challenging to interpret due to the complex interactions between climate and particulate transport across ocean margins. For the southern South China Sea over the last 90 thousand years, we observe a contrasting temporal relationship between the deposition of clay minerals (smectite) and magnetic minerals (hematite), which were associated with two different hydrodynamic modes. Fine-grained clay minerals can be carried in suspension by ocean currents, leading to a rapid response to regional climate-driven inputs. In contrast, changes in magnetic mineralogy were closely associated with bedload transport and resuspension linked to glacial-interglacial sea-level variability. Overall, this study indicates that the transfer pathways and mechanisms imparted by varying hydrodynamic conditions exert a substantial influence on the distribution of terrigenous material in continental shelf sediments.

Hosted file

`2. supporting information.docx` available at https://authorea.com/users/527622/articles/596675-contrasting-sensitivity-of-weathering-proxies-to-quaternary-climate-and-sea-level-fluctuations-in-the-southern-south-china-sea

Hosted file

`essoar.10507488.1.docx` available at https://authorea.com/users/527622/articles/596675-contrasting-sensitivity-of-weathering-proxies-to-quaternary-climate-and-sea-level-fluctuations-in-the-southern-south-china-sea

Contrasting sensitivity of weathering proxies to Quaternary climate and sea level fluctuations in the southern South China Sea

Yi Zhong [1, 2 3, 4], David J. Wilson [5], Jiabo Liu [1, 3, 4], Shiming Wan [6], Rui Bao [7], Jianxing Liu [8], Yanan Zhang [1], Xuesong Wang [2], Yuanhao Liu [1], Xiaoyu Liu [1], Ying Zhao [1], Qingsong Liu [1, 3, 4*]

[1] Center for Marine Magnetism (CM^2), Department of Ocean Science and Engineering, Southern University of Science and Technology, Shenzhen 518055, PR China

[2] Key Laboratory of Ocean and Marginal Sea Geology, South China Sea Institute of Oceanology, Chinese Academy of Sciences, Guangzhou 510301, China

[3] Laboratory for Marine Geology, Qingdao National Oceanography Laboratory for Marine Science and Technology, Qingdao 266061, China

[4] Southern Marine Science and Engineering Guangdong Laboratory (Guangzhou), Guangzhou, China

[5] Institute of Earth and Planetary Sciences, University College London and Birkbeck, University of London, London, UK

[6] Key laboratory of Marine Geology and Environment, Institute of Oceanology, Chinese Academy of Sciences, Qingdao 266071, China

[7] Key Laboratory of Marine Chemistry Theory and Technology, Ministry of Education/Institute for Advanced Ocean Studies, Ocean University of China, Qingdao, China

[8] Key Laboratory of Marine Sedimentology and Environmental Geology, First Institute of Oceanography, Ministry of Natural Resources (MNR), Qingdao, China

*Corresponding author: `qsliu@sustech.edu.cn`

Key Points:

In the southern South China Sea, clay mineralogy responds rapidly to climate-driven changes in inputs on orbital timescales.

Magnetic content within the coarser fraction is more strongly influenced by sea-level change, through bedload and resuspension transport.

This depositional framework may serve as a guideline for evaluating sea-level change on continental shelves over orbital timescales.

Abstract

Tropical marginal seas host unique sedimentary archives that may be exploited to reveal past changes in continental erosion, chemical weathering, and ocean dynamics. However, these records can be challenging to interpret due to the complex interactions between climate and particulate transport across ocean margins. For the southern South China Sea over the last 90 thousand years, we observe a contrasting temporal relationship between the deposition of clay minerals (smectite) and magnetic minerals (hematite), which were associated with two different hydrodynamic modes. Fine-grained clay minerals can be carried in suspension by ocean currents, leading to a rapid response to regional climate-driven inputs. In contrast, changes in magnetic mineralogy were closely associated with bedload transport and resuspension linked to glacial-interglacial sea-level variability. Overall, this study indicates that the transfer pathways and mechanisms imparted by varying hydrodynamic conditions exert a substantial influence on the distribution of terrigenous material in continental shelf sediments.

Plain Language Summary

Sediments that accumulate in the ocean along continental margins contain the minerals that were eroded and transported by rivers on the nearby land masses. Past changes in the composition of such sediments can be used to reconstruct the history of physical erosion and chemical weathering on the nearby landmasses, but can also be affected by ocean dynamics over orbital and millennial timescales. Here, clay mineralogy, sediment grain size, and rock magnetic signatures were measured in a core from the continental slope of the southern South China Sea, spanning the last 90 thousand years. Differences between the clay mineral and magnetic records, which are linked to finer and coarser sediment fractions respectively, indicate that specific mechanisms and timescales influenced sediment transport to the core site. This depositional framework must be considered when interpreting the timing of changes in weathering and erosion proxies hosted in sediment records from marginal seas. Specifically, fine-grained clay minerals may reveal a rapid response to weathering changes on the nearby continent, whereas the magnetic records are influenced by the transport of coarser-grained minerals under the influence of sea-level change. In addition, this framework could potentially serve as an indicator of past sea-level change on continental shelves.

Introduction

While continental margins and marginal seas account for only ~10-20% of the global ocean area, many are located in highly dynamic regions in which elevated physical erosion, chemical weathering, and organic carbon burial play a major role in the global carbon cycle (Wan et al., 2009). Moreover, continen-

tal margins are characterised by rapid sediment accumulation, such that high-resolution records of past weathering and erosion can potentially be obtained by deciphering the geochemical and mineralogical signatures within these sedimentary successions. Hence, these regions are of great strategic value for research into continent-ocean interactions and paleoclimate variations over millennial and orbital timescales (Wan et al., 2017; Xu et al., 2021). However, a detailed understanding of the controls on sediment transport, deposition, and burial in these complex environments is a prerequisite for interpreting these sedimentary records and recognizing their implications for the global carbon cycle (Wan et al., 2012; Xu et al., 2018).

Due to their physico-chemical properties, such as mineral surface area and cation exchange capacity, terrestrial minerals play a crucial role in governing the amount and type of organic matter ultimately preserved in ocean sediments (Blattmann et al., 2019). Moreover, particle resuspension and lateral advection of sediment (Quaresma et al., 2007) within nepheloid layers (Oliveira et al., 2002) may generate disparities in the spatial distribution of terrestrial minerals with differing grain-size associations due to hydrodynamic sorting (Ohkouchi et al., 2002; Thomsen & Gust, 2000). Therefore, in the Chinese marginal seas, terrigenous organic carbon transport, distribution, and preservation are largely determined by hydrodynamic sorting processes (Bao et al., 2018). However, the impact of these processes on interpretations of paleoclimate and weathering signals documented in sediment records from the marginal seas is less well understood.

Climate fluctuations during Quaternary glacial-interglacial cycles have significantly influenced the flux and composition of terrigenous sediment supplied to continental shelves, slopes, and deep-sea basins, modulated both by changes in precipitation and runoff and by sea-level fluctuations (Griffiths et al., 2009; Steinke et al., 2008). For examples, studies based on clay mineralogy and sediment geochemistry in the tropical marginal seas (e.g. Arabian Sea, Bay of Bengal, and South China Sea) revealed increases in terrigenous detrital input, organic carbon burial, and marine productivity during glacial periods, which was linked to the exposure of continental shelves (Xu et al., 2020; 2021). Because of the association of different terrigenous minerals with different sedimentary grain-size fractions (Bao et al., 2019), definitive evidence for such a sea-level hypothesis could be obtained through targeted investigations at the mineral grain-size level which would enable attribution to hydrodynamic sorting.

The southern South China Sea (SCS), together with the wide Sunda Shelf, is suitable for exploring the effects of sea-level change on terrigenous sediment input because this region receives large fluvial sediments fluxes and has been dramatically influenced by sea-level rise during the deglacial and early Holocene periods (Figure 1) (Hanebuth & Stattegger, 2004; Hanebuth et al., 2002; Milliman et al., 1999). Here, we compare grain size, clay mineralogy, and magnetic mineralogy records from the southern SCS over the last 90 kyr in order to assess the prevalence and nature of hydrodynamic mineral-sorting influences on

the sedimentary archive. Our findings underscore an important link between regional hydrodynamics and the depositional patterns of weathering and erosion indicators in the marginal seas.

Materials and methods

The studied sediment core HYIV2015-B9 (hereafter referred to as B9; 10.2484°N, 112.7325°E; 2603 m water depth) was retrieved from the northern slope of Nasha Terrace in the southern SCS (Figure 1) during cruise HYIV20150816 of *R/V Haiyang IV* in 2015. The core is 4.25 m long and is dominated by homogenous dark grey clay without visible bioturbation. The age model for core B9 was constrained by 9 AMS ^{14}C dates of planktonic foraminifera in the upper part (< 170 cm) (Li et al., 2018a) (Figure S1 and S2). The chronology for the deeper part was established in this study by correlating the benthic foraminiferal *C. wuellerstorfi* ^{18}O record to the LR04 benthic foraminiferal ^{18}O stack (Lisiecki & Raymo, 2005), supported by variations in the elemental Ca/Al ratios in core B9 where the benthic ^{18}O record was less well resolved (Figure S1 and S2; Text S2 in the supporting information). Overall, the core provides a continous sedimentary record extending from the Holocene back to early mainre isotope stage (MIS) 5 (~90 ka BP), with sedimentation rates varying from 1.8 to 7.3 cm/kyr (Text S2 in the supporting information).

For foraminiferal oxygen and carbon isotope measurements, epifaunal benthic foraminifera *Cibicidoides wuellerstorfi* were picked from the >250 m size fraction at 2 to 4 cm intervals, and ^{13}C and ^{18}O values were measured on a Thermo Scientific MAT 253 mass spectrometer, with calibration to the PDB standard. For the elemental analysis, approximately 2-g freeze-dried sediments were taken at 1 to 4 cm intervals and crushed into powder. Following digestion in a mixture of HF and HNO_3, major element abundances were determined using ICP-OES (IRIS Intrepid II XSP) following the methodology of Qi et al. (2000). The accuracy of this method, determined by analysing standard reference materials (Chinese marine sediments GBW 07315 and GBW 07316, and U.S. Geological Survey basalt BHVO-2), is better than 3%. A total of 225 samples were taken at 2-cm intervals to perform grain size, clay mineralogical composition, and rock magnetic analysis. More detailed information on the analytical methods is provided in Text S1 in the supporting information.

3. Results and Discussions

3.1. Provenance discrimination

The relative abundance of clay minerals in marine sediment records can provide information on the erosional sources in the hinterland and, to some extent, on climate variability (Steinke et al., 2008). Interpreting such records requires a detailed knowledge of the potential source areas, but also the mode and strength

of transport processes (Liu et al., 2010; Wan et al., 2010a). Since eolian fluxes in the southern SCS are low (Liu et al., 2004), terrigenous sediments in this region are mainly delivered by the surrounding rivers, such as the Mekong River and rivers from Borneo, Sumatra, the Malay Peninsula, and Thailand (Huang et al., 2016; Liu et al., 2015) (Figure 1 and 2; see also Text S3). Most of the Sunda Shelf sediments were originally supplied by the Mekong River and North Borneo rivers, with these supply routes confirmed by the presence of glacial-aged incised valleys across the Sunda Shelf (Schimanski & Stattegger, 2005) and offshore of the modern Mekong River (Tjallingii et al., 2010).

In order to interpret sediment provenance in core B9, its clay mineral assemblages are compared to these potential riverine sources in a ternary diagram (Figure 2). In the absence of distinct overlap between these data and the Mekong, northern Borneo, or other potential sources, it appears that a mixture of sources influenced the slope area of the Sunda Shelf. The clay mineral compositions in core ODP 1143 (Wan et al., 2017) also plot quite close to the data from core B9 (Figure 2), which suggests that both cores are influenced by a mixture of sediment sources from the Mekong River, North Borneo, and the Sunda Shelf. We further infer that the Mekong River, with its high illite and chlorite content, has been the predominant source of clay minerals to core B9 (Figure 2). Such findings are also supported by previous studies from nearby cores, namely SO18383-3 (Jiwarungrueangkul et al., 2019a) and CG2 (Huang et al., 2016) (Figure 2), which also indicate the Mekong River as a primary sediment source.

Hematite minerals are ubiquitous in the Mekong River and can make a significant contribution to deposits in the Southern SCS basin (e.g. Kissel et al., 2016, 2018). Given the significantly weaker magnetization of hematite than magnetite, the low S-ratios and HIRM values indicate the presence of abundant hematite in core B9 (Figure S4). In addition, consistent magnetic properties across glacial-interglacial cycles (Figure S5) probably imply a relatively stable sediment provenance. Together with clay mineralogical analysis (Figure 2), our rock magnetic results support the Mekong River as a major stable sediment source for core B9.

3.2. Spatial and temporal heterogeneity of depositional processes

Climate is a principal controlling factor of chemical weathering intensity over millennial to orbital timescales, while other driving factors include regional tectonics (Dixon et al., 2012), rock mineralogy (Babechuk et al., 2014), vegetation distribution (Galy et al., 2008), and geomorphology (Bouchez et al., 2012). For the SCS, its geographic extension over different, monsoon-controlled climatic regions (Chen et al., 2017), as well as the geological and geomorphological heterogeneity of the river catchments, also leads to a clear differentiation of sediment particles being delivered to the basin (Clift et al., 2015). As such, differences in both the terrigenous sediment supply in reponse to climate variability and the

local depositional processes may be expected between the northern and southern continental margins.

Our high-resolution record from core B9 on the southern margin of the SCS resolves climate signals over both orbital and sub-orbital timescales (Figure 3 and S3). The smectite/(illite + chlorite) ratio (Figure 3e) exhibits similar patterns to variations in the northern SCS (Zhao et al., 2018) (Figure 3d), which were controlled by the intensity of the East Asian summer monsoon (EASM) (Cheng et al., 2016) (Figure 3c). In the northen SCS, rapid increases in the smectite/(illite + chlorite) ratio (Figure 3d) suggest a fast response to strengthened EASM rainfall (Figure 3c), which varied coincident with both precessional-scale orbital forcing (Figure 3b) and Dansgaard-Oeschger (DO) and Bølling-Allerød (BA) interstadials (North Greenland Ice Core Project Members, 2004) (Figure 3a). Millennial-scale oscillations in clay mineralogy driven by the EASM intensity are also present in our southern SCS record, but cannot be so clearly resolved because of its lower sedimentation rate (Figure 3e), while this variability is superimposed on a clear precessional variability. Precessional fluctuations in chemical weathering indicators have previously been observed in both the southern and northern SCS (Chen et al., 2017), consistent with precessional changes in the EASM (Figure 3b). In general, a 23 kyr periodicity in the smectite/(illite + chlorite) ratio in phase with precession-driven insolation indicates that the response of clay mineralogy in the low-latitude SCS to the prevailing EASM arises rapidly and mainly through changing chemical weathering intensity (Li et al., 2018b; Zhao et al., 2018).

It has also been shown that variations in two iron oxide/oxyhydroxide minerals, hematite (-Fe_2O_3) and goethite (-FeOOH), could provide a useful weathering proxy (Zhang et al., 2007). Apart from erosion of bedrock sources such as red sandstones, hematite forms either through strong hydrolysis (i.e. lateritic soils) or from dehydration of goethite (Lepre & Olsen, 2021). During silicate weathering, the formation of hematite and goethite are competitive, with dry and warm climates favoring hematite, and wet and cool climates forming goethite (Ji et al., 2004). Previous studies on rock magnetic data from cores in the northern SCS have found that some high-coercivity minerals, such as hematite coeval with maghemite (Figure 3h), originate from vigorous chemical weathering (Yang et al., 2016). However, in general, sediment in that region is largely supplied from Taiwan and the Pearl River, with high and stable magnetite contents relative to hematite (Kissel et al., 2016, 2017). The low hematite content in the northern SCS coincides with coarse magnetic mineral grain size (i.e. low ARM/SIRM) (Figure 3i), consistent with high susceptibility values, reflecting intensified physical erosion and strong transport of coarse grains. At times, such as during the Holocene and late MIS 3, those low hematite contents and coarse grain sizes also coincide with oxygen isotope values for stalagmites (Cheng et al., 2016) (Figure 3c) and sea surface temperature (SST) reconstructions (Wei et al., 2007) (Figure 3j) that indicate a warm climate and strong EASM.

Interestingly, the hematite-rich intervals in core B9 (Figure 3k) are characterised

by a coarse magnetic grain size in the southern SCS (Figure 3g), and are coincident with coarse magnetic grain sizes but low hematite contents in the northern SCS (Figure 3h, i). Furthermore, the hematite content shows a clear 23 kyr periodicity, but opposite in phase to the variations in the smectite/(illite + chlorite) ratio in core B9 (Figure 3e, k). In the northern SCS, the depositional processes mean that enhanced hematite content (inferred from magnetic records) may be interpreted as a signature of high weathering intensity (Yang et al., 2016). In contrast, the inverse behaviour of the hematite/(goethite+hematite) fluctuations in the southern SCS indicates a different control, which we suggest arises from the interaction between the Mekong River and global sea-level change (Figure 3m). A large decrease in the S-ratio during glacial periods (Figure 3l) and the presence of high-coercivity minerals (Figure S5) further support increased hematite contents that may have been originally derived from Mekong River inputs. The close coincidence between magnetic grain-size variations (Figure 3g) and sediment coarsening (Figure 3f) in core B9, which is particularly evident during the Last Glacial Maximum (LGM), supports the hypothesis of a transport-driven control, which is further explored in the next section.

3.3. Differential hydrodynamic influences on terrigenous sediments in the southern SCS

Differential transport and depositional dynamics among grain-size classes may provide explanations for discrepancies in timing between weathering proxies measured at continental margin sites (Magill et al., 2018). Such hydrodynamic effects, as well as degradation during transport, could represent an intrinsic function that accounts for proxy paradoxes (Epping et al., 2002; McCave & Hall, 2006; Mulder et al., 2013). It is important to note that sorting processes can also lead to differential impacts within a grain-size fraction, due to differences in properties such as particle sphericity, particle aggregation, matrix association, or mineralogy (Blattmann et al., 2019; McCave & Hall, 2006; Tesi et al., 2016).

Sea-level change and global and regional climate can lead to varying hydrodynamic influences on terrigenous inputs and transport in the SCS (Colin et al., 2010; Huang et al., 2019; Jiwarungrueangkul et al., 2019). Here we suggest that the inverse relationship between clay mineral and magnetic mineral tracers of weathering intensity in the southern SCS in response to the EASM (Figure 3) provides an example of such a hydrodynamic influence. The siliciclasic grain size measurements (Figure S6) indicate a robust correlation between the variation of the fine grain size (4 m) (Figure 3f) and the magnetic grain sizes (Figure 3g), with coarser grain sizes occuring during intervals of lower sea level (Figure 3m) and hence closer proximity to the Mekong River mouth (Figure 1).

During interglacial periods, when sea level was higher, the strong EASM led to heavy rainfall and high river runoff (Figure 4a). Under these conditions, strong erosion and weathering in the hinterland would have provided an abundant supply of smectite and hematite to the Sunda Shelf (Wan et al., 2017; Zhang et al., 2007). Previous studies have indicated that suspended load and bedload trans-

port can lead to differential transport between the finer and coarser fractions, as recorded by changes in the radiocarbon content of sedimentary organic matter (Bao et al., 2019). Despite the longer transport distance from the Sunda Shelf to the deeper regions of the SCS at these times, fine-grained smectites could be transported in nepheloid layers (Gao & Collins, 2014; Zhu et al., 2006). As such, the clay mineral record is able to express climate-driven changes in weathering inputs driven by the EASM, although potentially further influenced by surface and intermediate water dynamics.

In contrast, since coarser-grained sediments are less liable to rapid seaward transport under such hydrodynamic conditions (Gao & Collins, 2014; Zhu & Chang, 2000), hematite within the coarser grain size fractions would mostly be deposited proximally on the continental shelf (Figure 4a). Similarly, sluggish across-shelf bedload transport was observed to be accompanied by the selective degradation of organic carbon in coarser grain size fractions and a pronounced ^{14}C aging of the residual organic matter (Bao & Blattmann, 2020). As such, despite rapid formation of hematite and/or its enhanced export by rivers under conditions of a strong EASM, the amount of hematite reaching the deep sea would have been limited.

The operation of such transport processes in shallow shelf regions could change with glacial-interglacial changes in sea level (Zhang et al., 2021), leading to enhanced hematite export associated with coarser-grained sediments during glacial periods (Figure 4b). Specifically, with a fall in sea level, the position of core B9 would have been closer to the paleo-Mekong River mouth, enabling the transport of silt-sized sediments to the site, primarily from the exposed Sunda Shelf (Figure 1c). The silt-sized sediments could also reflect reworking, during periods of low sea level, of the coarse detrital material that was previously deposited on the Sunda Shelf. As such, enhanced deposition of hematite during glacial periods could reflect weathering conditions from the previous (or earlier) interglacial periods, and does not provide a robust indicator of weathering intensity or fluxes coincident with its deposition. Overall, this observation provides an important demonstration that hydrodynamic processes play an important role in shaping the spatial and temporal distribution of mineralogical and geochemical indicators of chemical weathering in the hinterland, and must be considered before interpreting such changes directly in terms of carbon cycle changes.

4. Conclusions

Contrasting depositional patterns among proxies hosted by different grain-size classes in sediments of the southern South China Sea over the last 90 kyr indicate the effect of differential transport dynamics by suspension and bedload transport. Fluctuations in smectite/(illite + chlorite) ratios correlate with the East Asian Summer Monsoon intensity and were associated with an intensification of erosion and chemical weathering in the tropical hinterland. In contrast, hematite content in the coarser fractions was subject to the influence of global

sea level change and hydrodynamic sorting, which restricted its delivery to deep sea settings until sea level fell during glacial periods. These results indicate that sea level dynamics may be responsible for creating lead-lag patterns (or antiphasing) between proxies with similar climatic or provenance controls but contained in differing grain-size classes. As such, these differential hydrodynamic influences are important factors to consider in interpretations of diverse multi-proxy down-core records, in particular when considering millennial and orbital-scale weathering and paleoclimate signals contained in terrigenous continental margin sequences.

Acknowledgements

References

Babechuk, M. G., Widdowson, M., & Kamber, B. S. (2014). Quantifying chemical weathering intensity and trace element release from two contrasting basalt profiles, Deccan Traps, India. *Chemical Geology*, 363, 56-75.

Bao, R., & Blattmann, T. M. (2020). Radiocarbonscapes of Sedimentary Organic Carbon in the East Asian Seas. *Frontiers in Marine Science*, 7, 517.

Bao, R., Blattmann, T. M., McIntyre, C., Zhao, M., & Eglinton, T. I. (2019). Relationships between grain size and organic carbon ^{14}C heterogeneity in continental margin sediments. *Earth and Planetary Science Letters*, 505, 76-85.

Bao, R., McIntyre, C., Zhao, M., Zhu, C., Kao, S. J., & Eglinton, T. I. (2016). Widespread dispersal and aging of organic carbon in shallow marginal seas. *Geology*, 44, 791-794.

Bao, R., Uchida, M., Zhao, M., Haghipour, N., Montlucon, D., McNichol, A., et al. (2018). Organic Carbon Aging During Across-Shelf Transport. *Geophysical Research Letters*, 45, 8425-8434.

Berger, A. L. (1978). Long-Term Variations of Caloric Insolation Resulting from the Earth's Orbital Elements. *Quaternary Research*, 9(2), 139-167.

Blattmann, T. M., Liu, Z., Zhang, Y., Zhao, Y., Haghipour, N., Montlucon, D. B., et al. (2019). Mineralogical control on the fate of continentally derived organic matter in the ocean. *Science*, 366, 742-745.

Bouchez, J., Gaillardet, J., Lupker, M., Louvat, P., France-Lanord, C., Maurice, L., et al. (2012). Floodplains of large rivers: Weathering reactors or simple silos? *Chemical Geology*, 332, 166-184.

Chen, Q., Kissel, C., & Liu, Z. (2017). Late Quaternary climatic forcing on the terrigenous supply in the northern South China Sea: Input from magnetic studies. *Earth and Planetary Science Letters*, 471, 160-171.

Cheng, H., Edwards, R. L., Sinha, A., Spötl, C., Yi, L., Chen, S., et al. (2016). The Asian monsoon over the past 640,000 years and ice age terminations. *Nature*, 534, 640-646.

Clift, P. D., Brune, S., & Quinteros, J. (2015). Climate changes control offshore crustal structure at South China Sea continental margin. *Earth and Planetary Science Letters*, 420, 66-72.

Colin, C., Siani, G., Sicre, M. A., & Liu, Z. (2010). Impact of the East Asian monsoon rainfall changes on the erosion of the Mekong River basin over the past 25,000yr. *Marine Geology*, 271, 84-92.

Dixon, J. L., Hartshorn, A. S., Heimsath, A. M., DiBiase, R. A., & Whipple, K. X. (2012). Chemical weathering response to tectonic forcing: A soils perspective from the San Gabriel Mountains, California. *Earth and Planetary Science Letters*, 323, 40-49.

Epping, E., van der Zee, C., Soetaert, K., & Helder, W. (2002). On the oxidation and burial of organic carbon in sediments of the Iberian margin and Nazare Canyon (NE Atlantic). *Progress in Oceanography*, 52, 399-431.

Galy, V., Francois, L., France-Lanord, C., Faure, P., Kudrass, H., Palhol, F., Singh, S. K. (2008). C4 plants decline in the Himalayan basin since the Last Glacial Maximum. *Quaternary Science Reviews*, 27, 1396-1409.

Gao, S., & Collins, M. B. (2014). Holocene sedimentary systems on continental shelves. *Marine Geology*, 352, 268-294.

Griffiths, M. L., Drysdale, R. N., Gagan, M. K., Zhao, J. X., Ayliffe, L. K., Hellstrom, J.C., et al. (2009). Increasing Australian–Indonesian monsoon rainfall linked to early Holocene sea-level rise. *Nature Geoscience*, 2, 636-639.

Hanebuth, T. J. J., Stattegger, K. (2000). Rapid flooding of the Sunda Shelf: A late-glacial sea-level record. *Science*, 288(5468), 1033-1035.

Hanebuth, T. J. J., & Stattegger, K. (2004). Depositional sequences on a late Pleistocene–Holocene tropical siliciclastic shelf (Sunda Shelf, southeast Asia).

Journal of Asian Earth Sciences, 23, 113-126.

Hanebuth, T. J. J., Stattegger, K., & Saito, Y. (2002). The stratigraphic architecture of the central Sunda Shelf (SE Asia) recorded by shallow-seismic surveying. *Geo-Marine Letters*, 22, 86-94.

Huang, J., Wan, S., Li, A., & Li, T. (2019). Two-phase structure of tropical hydroclimate during Heinrich Stadial 1 and its global implications. *Quaternary Science Reviews*, 222, 105900.

Huang, J., Wan, S., Xiong, Z., Zhao, D., Liu, X., Li, A., & Li, T. (2016). Geochemical records of Taiwan-sourced sediments in the South China Sea linked to Holocene climate changes. *Palaeogeography, Palaeoclimatology, Palaeoecology*, 441, Part 4, 871-881.

Ji, J., Chen, J., Balsam, W., Lu, H., Sun, Y., & Xu, H. (2004). High resolution hematite/goethite records from Chinese loess sequences for the last glacial-interglacial cycle: Rapid climatic response of the East Asian Monsoon to the tropical Pacific. *Geophysical Research Letters*, 31, 347-348.

Jiwarungrueangkul, T., Liu, Z., & Zhao, Y. (2019). Terrigenous sediment input responding to sea level change and East Asian monsoon evolution since the last deglaciation in the southern South China Sea. *Global and Planetary Change*, 174, 127-137.

Kissel, C., Liu, Z., Li, J., & Wandres, C., 2016. Magnetic minerals in three Asian rivers draining into the South China Sea: Pearl, Red, and Mekong Rivers. *Geochemistry, Geophysics, Geosystems*, 17, 1678-1693.

Kissel, C., Liu, Z., Li, J., & Wandres, C. (2017). Magnetic signature of river sediments drained into the southern and eastern part of the South China Sea (Malay Peninsula, Sumatra, Borneo, Luzon and Taiwan). *Sedimentary Geology*, 347, 10-20.

Lepre, C. J., & Olsen, P. E. (2021). Hematite reconstruction of Late Triassic hydroclimate over the Colorado Plateau. *Proceedings of the National Academy of Sciences*, 118, e2004343118.

Li, G., Rashid, H., Zhong, L., Xu, X., Yan, W., & Chen, Z. (2018a). Changes in Deep Water Oxygenation of the South China Sea Since the Last Glacial Period. *Geophysical Research Letters*, 45, 9058-9066.

Li, M., Ouyang, T., Tian, C., Zhu, Z., Peng, S., Tang, Z., et al. (2018b). Sedimentary responses to the East Asian monsoon and sea level variations recorded in the northern South China Sea over the past 36 kyr. *Journal of Asian Earth Sciences*, 171, 213-224.

Lisiecki, L. E., & Raymo, M. E. (2005). A Pliocene-Pleistocene stack of 57 globally distributed benthic ^{18}O records. *Paleoceanography*, 20, PA1003.

Liu, J. P., Milliman, J. D., Gao, S., & Cheng, P. (2004). Holocene development of the Yellow River's subaqueous delta, North Yellow Sea. *Marine Geology*,

209(1-4), 45-67.

Liu, Z., Colin, C., Trentesaux, A., Blamart, D., Bassinot, F., Siani, G., & Sicre, M. A. (2004). Erosional history of the eastern Tibetan Plateau since 190 kyr ago: Clay mineralogical and geochemical investigations from the southwestern South China Sea. *Marine Geology*, 209, 1-18.

Liu, Z., Colin, C., Li, X., Zhao, Y., Tuo, S., Chen, Z., et al. (2010). Clay mineral distribution in surface sediments of the northeastern South China Sea and surrounding fluvial drainage basins: Source and transport. *Marine Geology*, 277, 48-60.

Liu, Z., Zhao, Y., Colin, C., Stattegger, K., Wiesner, M. G., Huh, C. A., et al. (2015). Source-to-Sink transport processes of fluvial sediments in the South China Sea. *Earth-Science Reviews*, 153, 238-273.

Magill, C. R., Ausin, B., Wenk, P., McIntyre, C., Skinner, L., Martinez-Garcia, A., et al. (2018). Transient hydrodynamic effects influence organic carbon signatures in marine sediments. *Nature Communications*, 9, 4690.

McCave, I. N., & Hall, I. R. (2006). Size sorting in marine muds: Processes, pitfalls, and prospects for paleoflow-speed proxies. *Geochem. Geophys. Geosyst*, 7, Q10N05.

Milliman, J. D., Farnsworth, K. L., & Albertin, C. S. (1999). Flux and fate of fluvial sediments leaving large islands in the East Indies. *Journal of Sea Research*, 41, 97-107.

Milliman, J. D., & Farnsworth, K. L. (2011). River Discharge to the Coastal Ocean: A Global Synthesis. Cambridge University Press.

Mulder, T., Hassan, R., Ducassou, E., Zaragosi, S., Gonthier, E., Hanquiez, V., et al. (2013). Contourites in the Gulf of Cadiz: a cautionary note on potentially ambiguous indicators of bottom current velocity. *Geo-Marine Letter*s, 33, 357-367.

North Greenland Ice Core Project members. (2004). High-resolution record of Northern Hemisphere climate extending into the last interglacial period. *Nature*, 431, 147-151.

Ohkouchi, N., Eglinton, T. I., Keigwin, L. D., & Hayes, J. M. (2002). Spatial and temporal offsets between proxy records in a sediment drift. *Science*, 298, 1224-1227.

Oliveira, A., Vitorino, J., Rodrigues, A., Jouanneau, J. M., Dias, J. A., & Weber, O. (2002). Nepheloid layer dynamics in the northern Portuguese shelf. *Progress in Oceanography*, 52, 195-213.

Qi, L., Hu, J., & Gregoire, D. C. (2000). Determination of trace elements granites by inductively coupled plasma mass spectrometry. *Talanta*, 51(3), 507-513.

Quaresma, L. S., Vitorino, J., Oliveira, A., & da Silva, J. C. B. (2007). Evidence of sediment resuspension by nonlinear internal waves on the western Portuguese mid-shelf. *Marine Geology*, 246, 123-143.

Rohling, E. J., Liu, Q. S., Roberts, A. P., Stanford, J. D., Rasmussen, S. O., Langen, P. L., & Siddall, M. (2009). Controls on the East Asian monsoon during the last glacial cycle, based on comparison between Hulu Cave and polar ice-core records. *Quaternary Science Reviews*, 28, 3291-3302.

Schimanski, A., & Stattegger, K. (2005). Deglacial and Holocene evolution of the Vietnam shelf: stratigraphy, sediments and sea-level change. *Marine Geology*, 214, 365-387.

Steinke, S., Hanebuth, T. J., Vogt, C., & Stattegger, K. (2008). Sea level induced variations in clay mineral composition in the southwestern South China Sea over the past 17,000 yr. *Marine Geology*, 250, 199-210.

Tesi, T., Semiletov, I., Dudarev, O., Andersson, A., & Gustafsson, O. (2016). Matrix association effects on hydrodynamic sorting and degradation of terrestrial organic matter during cross-shelf transport in the Laptev and East Siberian shelf seas. *Journal of Geophysical Research-Biogeosciences*, 121, 731-752.

Thomsen, L., & Gust, G. (2000). Sediment erosion thresholds and characteristics of resuspended aggregates on the western European continental margin. *Deep-Sea Research Part I-Oceanographic Research Papers*, 47, 1881-1897.

Tjallingii, R., Stattegger, K., Wetzel, A., & Van Phach, P. (2010). Infilling and flooding of the Mekong River incised valley during deglacial sea-level rise. *Quaternary Science Reviews*, 29, 1432-1444.

Wan, S., Clift, P.D., Li, A., Yu, Z., Li, T., & Hu, D. (2012). Tectonic and climatic controls on long-term silicate weathering in Asia since 5 Ma. *Geophysical Research Letters*, 39, L15611.

Wan, S., Clift, P. D., Zhao, D., Hovius, N., Munhoven, G., France-Lanord, C., et al. (2017). Enhanced silicate weathering of tropical shelf sediments exposed during glacial lowstands: A sink for atmospheric CO_2. *Geochimica et Cosmochimica Acta*, 200, 123-144.

Wan, S., Kurschner, W. M., Clift, P. D., Li, A., & Li, T. (2009). Extreme weathering/erosion during the Miocene Climatic Optimum: Evidence from sediment record in the South China Sea. *Geophysical Research Letters*, 36, L19706.

Wan, S., Li, A., Clift, P. D., Wu, S., Xu, K., & Li, T. (2010a). Increased contribution of terrigenous supply from Taiwan to the northern South China Sea since 3Ma. *Marine Geology*, 278, 115-121.

Wan, S., Tian, J., Steinke, S., Li, A., & Li, T. (2010b). Evolution and variability of the East Asian summer monsoon during the Pliocene: Evidence from clay mineral records of the South China Sea. *Palaeogeography, Palaeoclimatology, Palaeoecology*, 293, 237-247.

Wang, Y. J., Cheng, H., Edwards, R. L., Kong, X. G., Shao, X. H., Chen, S. T., et al. (2008). Millennial- and orbital-scale changes in the East Asian monsoon over the past 224,000 years. *Nature*, 451, 1090-1093.

Wei, G. J., Deng, W. F., Liu, Y., & Li, X. H. (2007). High-resolution sea surface temperature records derived from foraminiferal Mg/Ca ratios during the last 260 ka in the northern South China Sea. *Palaeogeography, Palaeoclimatology, Palaeoecology*, 250(1), 126-138.

Wolff, E. W., Barbante, C., Becagli, S., Bigler, M., Boutron, C. F., Castellano, E., et al. (2010). Changes in environment over the last 800,000 years from chemical analysis of the EPICA Dome C ice core. *Quaternary Science Reviews*, 29, 285-295.

Xu, Z., Li, T., Clift, P. D., Wan, S., Qiu, X., & Lim, D. (2018). Bathyal records of enhanced silicate erosion and weathering on the exposed Luzon shelf during glacial lowstands and their significance for atmospheric CO_2 sink. *Chemical Geology*, 476, 302-315.

Xu, Z., Wan, S., Colin, C., Clift, P. D., Chang, F., Li, T., et al. (2021). Enhancements of Himalayan and Tibetan Erosion and the Produced Organic Carbon Burial in Distal Tropical Marginal Seas During the Quaternary Glacial Periods: An Integration of Sedimentary Records. *Journal of Geophysical Research-earth Surface*, 126, e2020JF005828.

Xu, Z., Wan, S., Colin, C., Li, T., Clift, P. D., Chang, F., et al. (2020). Enhanced terrigenous organic matter input and productivity on the western margin of the Western Pacific Warm Pool during the Quaternary sea-level lowstands: Forcing mechanisms and implications for the global carbon cycle. *Quaternary Science Reviews*, 232, 106211.

Yang, X., Peng, X., Qiang, X., Niu, L., Zhou, Q., & Wang, Y. (2016). Chemical Weathering Intensity and Terrigenous Flux in South China during the Last 90,000 Years—Evidence from Magnetic Signals in Marine Sediments. *Frontiers in Earth Science*, 4, 47.

Zhang, H., Li, D. W., Sachs, J. P., Yuan, Z., Wang, Z., Su, C., & Zhao, M. (2021). Hydrodynamic processes and source changes caused elevated ^{14}C ages of organic carbon in the East China Sea over the last 14.3 kyr. *Geochimica et Cosmochimica Acta*, 304, 347-363.

Zhang, Y. G., Ji, J., Balsam, W. L., Liu, L., & Chen, J. (2007). High resolution hematite and goethite records from ODP 1143, South China Sea: Co-evolution of monsoonal precipitation and El Niño over the past 600,000 years. *Earth & Planetary Science Letters*, 264, 136-150.

Zhao, S., Liu, Z., Colin, C., Zhao, Y. L., Wang, X. X., & Jian, Z. M. (2018). Responses of the East Asian Summer Monsoon in the Low-Latitude South China Sea to High-Latitude Millennial-Scale Climatic Changes During the Last

Glaciation: Evidence From a High-Resolution Clay Mineralogical Record. *Paleoceanography and Paloclimatology*, 33(7), 745-765.

Zhu, Y., & Chang, R. (2000). Preliminary study of the dynamic origin of the distribution pattern of bottom sediments on the continental shelves of the Bohai Sea, Yellow Sea and East China Sea. *Estuarine Coastal and Shelf Science*, 51, 663-680.

Zhu, Z. Y., Zhang, J., Wu, Y., & Lin, J. (2006). Bulk particulate organic carbon in the East China Sea: Tidal influence and bottom transport. *Progress in Oceanography*, 69, 37-60.

Zong, Y. (2004). Mid-Holocene sea-level highstand along the Southeast Coast of China. *Quaternary International*, 117(1), 55-67.
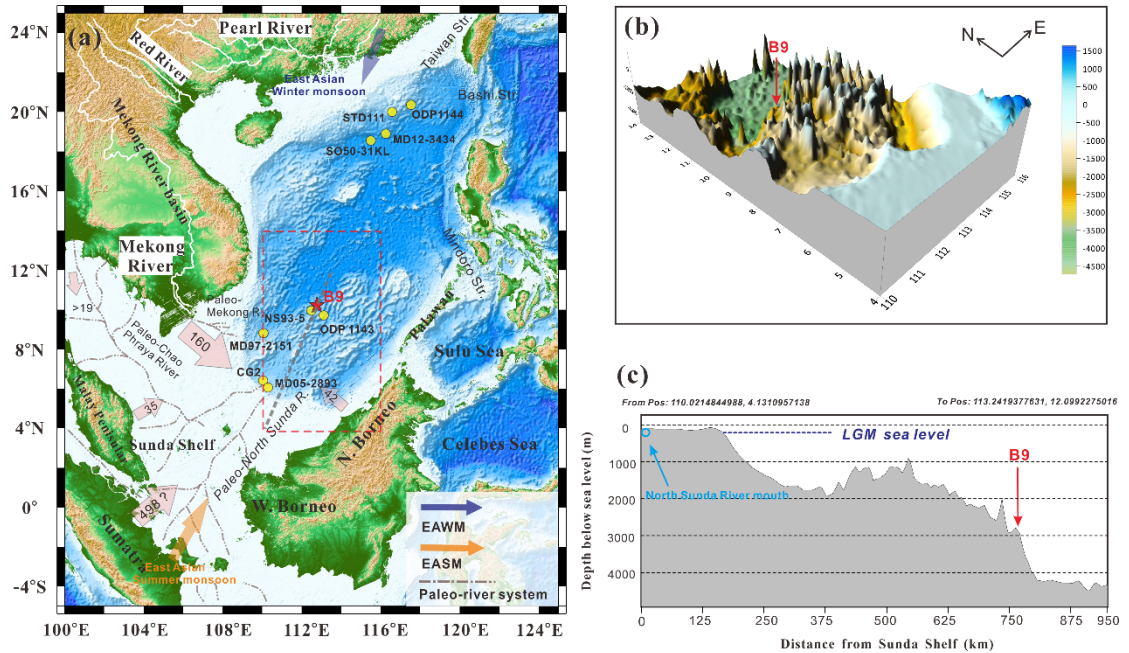
Figure captions:

Fig. 1

Figure 1. Geographic and bathymetric setting of the South China Sea. (a) Regional map showing the site of core B9 (red star), other referenced cores (yellow circles), topography, bathymetry, and modern and paleo-river systems. Large pink arrows with numbers represent annual sediment fluxes from major local sources in Mt/y, from Milliman and Farnsworth (2011). Arrows indicate modern near-surface Asian monsoon winds dominating during summer (EASM, orange) and winter (EAWM, blue). (b) Three-dimensional bathymetric map for

15

area marked in the red box in panel (a), showing bathymetric contours of the southern South China Sea. The topographic map was created by Surfer soft using ETOPO1 with 5 min precision. (c) Cross section, following grey dashed line in panel (a), indicating locations of the paleo-North Sunda river mouth, the studied core site (B9), and the approximate Last Glacial Maximum (LGM) sea level at ~130 m below present.
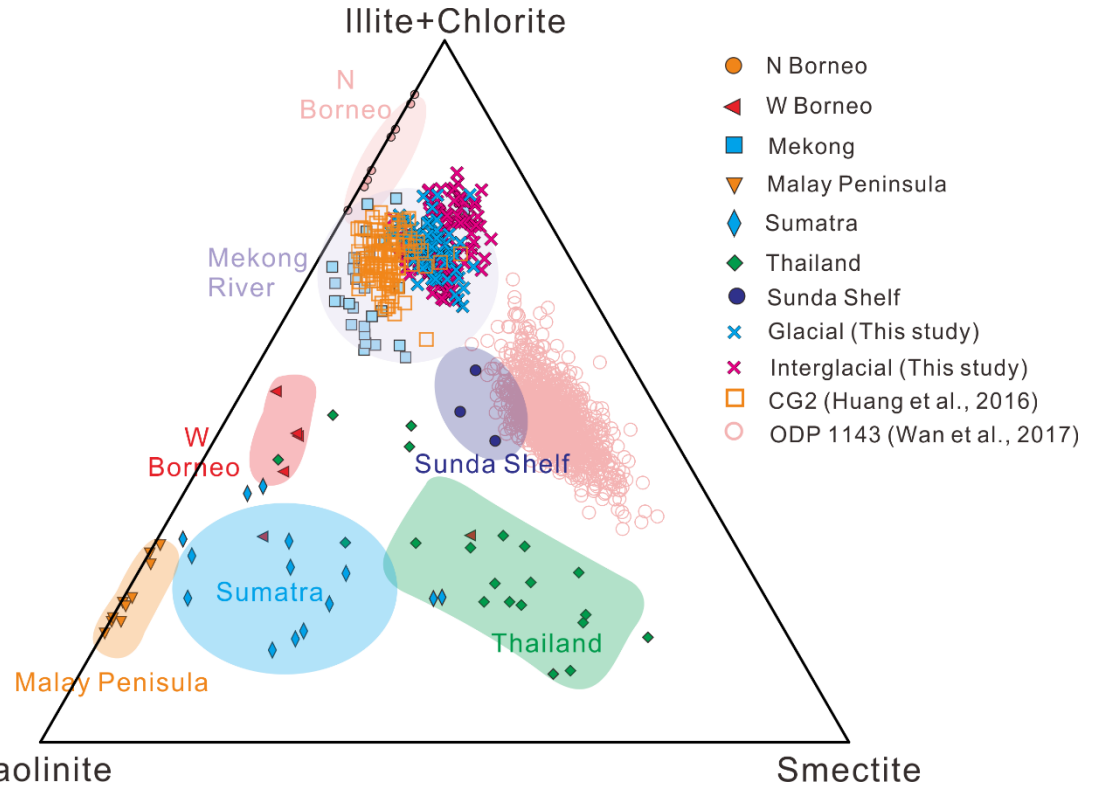

Fig. 2.

Figure 2. Ternary diagram of clay mineral assemblages in Core B9 and comparison to regional sources. Glacial and interglacial data from core B9 are shown with blue and red crosses, respectively. Potential sediment sources from surrounding rivers are indicated for comparison, including the Mekong River (Wan et al., 2010b) and Thailand (Chao Phraya) river systems in the Indochina Peninsula, river systems in Sumatra and the Malay Peninsula, and river systems in western (W) and northern (N) Borneo (Liu et al., 2007, 2012; Liu et al., 2016a, 2016b), and the Sunda Shelf (Wan et al., 2010b). Pleistocene data from cores CG2 (Huang et al., 2016) and ODP 1143 (Wan et al., 2017) are also shown for comparison.
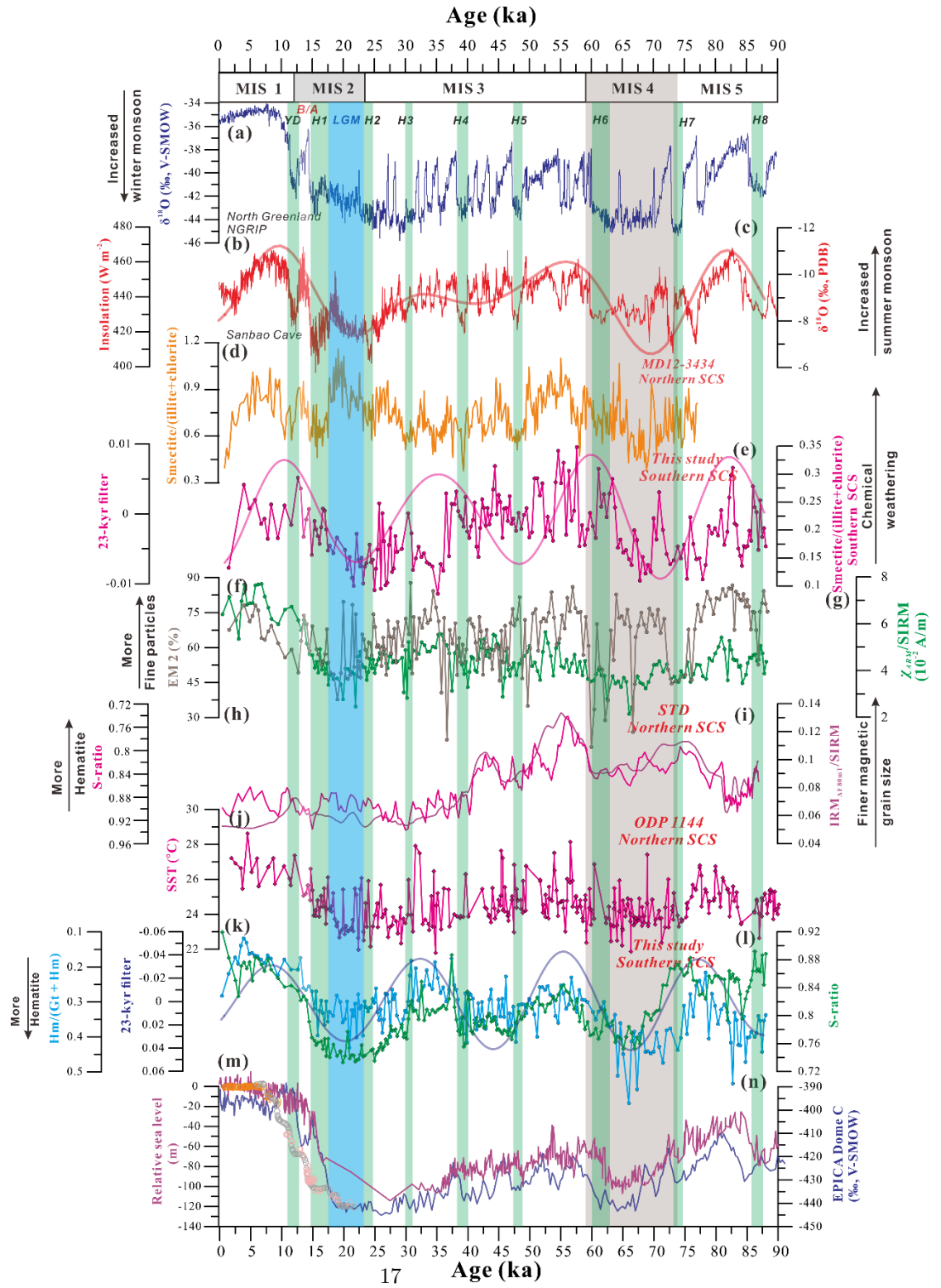
Fig. 3.

Age (ka)

0 5 10 15 20 25 30 35 40 45 50 55 60 65 70 75 80 85 90

| MIS 1 | MIS 2 | MIS 3 | MIS 4 | MIS 5 |

B/A
YD H1 LGM H2 H3 H4 H5 H6 H7 H8

(a) Increased winter monsoon

δ¹⁸O (‰, V-SMOW)

North Greenland NGRIP

(b) Insolation (W m⁻²)

Sanbao Cave

(c) δ¹⁸O (‰, PDB) Increased summer monsoon

(d) Smectite/(illite+chlorite)

MD12-3434 Northern SCS

(e) Smectite/(illite+chlorite) Southern SCS — Chemical weathering

23-kyr filter

This study Southern SCS

(f) EM 2 (%) — More Fine particles

(g) χ_ARM/SIRM (10⁻² A/m)

(h) S-ratio — More Hematite

STD Northern SCS

(i) IRM_{1.5-100 mT}/SIRM — Finer magnetic grain size

(j) SST (°C)

ODP 1144 Northern SCS

(k) Hm/(Gt + Hm) — More Hematite

23-kyr filter

This study Southern SCS

(l) S-ratio

(m) Relative sea level (m)

(n) EPICA Dome C (‰, V-SMOW)

17

Age (ka)

0 5 10 15 20 25 30 35 40 45 50 55 60 65 70 75 80 85 90

Figure 3. Proxy records from core B9 compared to other records over the past 90 kyr: (a) ^{18}O record from Greenland ice core (NGRIP Members, 2004); (b) 21 July insolation at 65°N (thick red curve; Berger, 1978); (c) stalagmite ^{18}O records from Hulu and Dongge Caves (Wang et al., 2008); (d) smectite/(illite + chlorite) ratio in core MD12-3434 in the northern SCS (Zhao et al., 2018); (e) smectite/(illite + chlorite) ratio in core B9 in the southern SCS (this study), and 23 kyr Gaussian bandpass filtered output (thick purple curve); (f, g) grain-size endmember EM2 and $_{ARM}$/SIRM in core B9 (this study); (h, i) S-ratio and IRM$_{AF80mT}$/SIRM ratio in core STD111 in the northern SCS (Yang et al., 2016); (j) sea surface temperature (SST) reconstruction from core ODP 1144 in the northern SCS (Wei et al., 2007); (k, l) hematite/(goethite + hematite) ratio (Hm/(Gt + Hm)) and S-ratio in core B9 in the southern SCS (this study), and 23 kyr Gaussian bandpass filtered output of Hm/(Gt + Hm) (thick blue line); (m) Relative sea level (RSL). Purple line represents global RSL (Rohling et al., 2009). Orange, grey, and pink dots represent RSL for the Southeast China Coast (Zong, 2004), East China Sea (Liu et al., 2004), and Sunda Shelf (Hanebuth et al., 2000), respectively. (n) D record from EPICA Dome C (Wolff et al., 2010). Grey bars indicate glacial intervals, blue bar indicates the last Glacial Maximum (LGM), and green bars indicate the Younger Dryas (YD) and Heinrich Stadials 1-8 (H1-8).
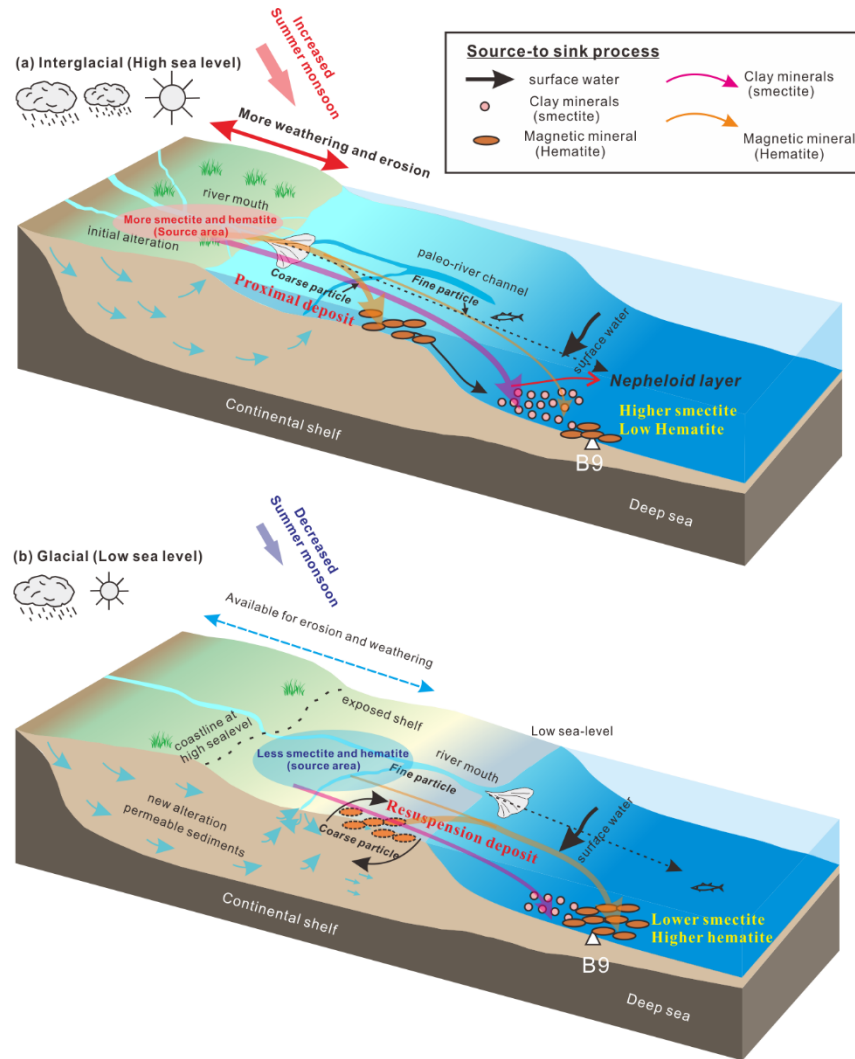
Fig. 4.

Figure 4. Conceptual model of processes that control the erosion, transport, and deposition of clays and magnetic minerals in marginal seas during (a) interglacials with high sea-level and (b) glacials with low sea-level. Figure is modified from Wan et al. (2017) based on new observations from this study.